Journal of Alloys and Compounds 680 (2016) 366–372

Contents lists available at ScienceDirect

Journal of Alloys and Compounds

journal homepage: http://www.elsevier.com/locate/jalcom

Superior electrochemical properties of SiO_2-doped Co_3O_4 hollow nanospheres obtained through nanoscale Kirkendall diffusion for lithium-ion batteries

Jong Min Won, Jung Sang Cho, Yun Chan Kang*

Department of Materials Science and Engineering, Korea University, Anam-Dong, Seongbuk-Gu, Seoul 136-713, Republic of Korea

ARTICLE INFO

Article history:
Received 6 January 2016
Received in revised form
9 April 2016
Accepted 12 April 2016
Available online 13 April 2016

Keywords:
Kirkendall diffusion
Cobalt oxide
Anode material
Lithium-ion battery
Flame spray pyrolysis

ABSTRACT

Hollow SiO_2-doped Co_3O_4 (Si–Co_3O_4) nanospheres with excellent Li-ion storage properties were synthesized via flame spray pyrolysis by applying a nanoscale Kirkendall diffusion process. A solid SiO_2-doped CoO (filled Si–CoO) nanopowder was prepared through this process, and then it was transformed into hollow Si–Co_3O_4 nanopowder by way of a core-shell-structured Co–SiO_2 (filled Co@Si–CoO) composite nanopowder. In addition, the direct oxidation of the filled Si–CoO nanopowder at 300 °C under an air atmosphere resulted in the formation of a solid SiO_2-doped Co_3O_4 (filled Si–Co_3O_4) nanopowder. At a high current density of 2 A g^{-1}, the hollow Si–Co_3O_4 nanospheres exhibited a 150th-cycle discharge capacity of 971 mA h g^{-1} and capacity retention of 99.5%, which was measured relative to the second cycle. However, the corresponding capacity retentions of the filled Si–CoO and Si–Co_3O_4 nanopowders were only 82.2% and 71.5%, respectively. The high structural stability during cycling and high Li-ion conductivity, which are caused by the hollow structure, are responsible for the excellent Li-ion storage properties of the hollow Si–Co_3O_4 nanospheres obtained through nanoscale Kirkendall diffusion.

© 2016 Elsevier B.V. All rights reserved.

1. Introduction

Cobalt oxides have been extensively studied because of their use in various applications, such as gas sensors, catalysts, magnetic materials, and energy-storage systems [1–18]. In addition, cobalt oxide nanostructures, such as nanopowders, nanorods, yolk-shells, hollow spheres, and nanotubes, have received significant attention as efficient anode materials for Li-ion batteries (LIBs) because of their high storage capacity; such materials can store more than eight Li atoms per formula unit [8–18]. However, the susceptibility of these materials to capacity fading, which is caused by pulverization during repeated Li insertion and desertion processes, remains a major drawback [19–23]. Therefore, a simple process for developing cobalt oxide nanostructures with improved Li-ion storage properties is needed.

Nanopowders with the desired stoichiometry can be directly prepared from a precursor solution composed of many elements by using a flame-assisted droplet-to-powder conversion process, which is commonly known as flame spray pyrolysis (FSP) [24–34]. Single and multi-component metal oxide nanopowders have been prepared through FSP for various applications, such as catalysts, gas sensors, phosphors, and magnetic materials [25–28]. The electrochemical properties of metal oxide nanopowders prepared via FSP have also been studied [29,30]. Furthermore, single-crystal metal oxide nanoparticles that are tens of nanometers in size can be formed from metal oxide vapors within the high-temperature diffusion flame at temperatures higher than 2500 °C [31]. However, the poor electrochemical properties of such nanopowders, including poor structural stability during cycling, rendered them inadequate as anode materials for LIBs [31–34].

Therefore, in this study, hollow SiO_2-doped Co_3O_4 (Si–Co_3O_4) nanospheres with 10 wt% of SiO_2 were prepared via FSP by applying a nanoscale Kirkendall diffusion process. SiO_2 was applied to avoid the aggregation of the metallic Co nanopowder during the post-treatment process under a reducing atmosphere. The resulting filled SiO_2-doped CoO (Si–CoO) nanopowder was transformed into hollow Si–Co_3O_4 nanospheres by way of a core-shell-structured Co–SiO_2 (filled Co@Si–CoO) composite nanopowder.

* Corresponding author.
E-mail address: yckang@korea.ac.kr (Y. Chan Kang).

http://dx.doi.org/10.1016/j.jallcom.2016.04.104
0925-8388/© 2016 Elsevier B.V. All rights reserved.

2. Experimental

The filled Si–CoO nanopowder was prepared from the vapors of cobalt oxide and silicon oxide through a one-pot FSP process. The FSP system used was composed of a droplet generator, flame nozzle, quartz reactor, powder collector, and blower. A schematic diagram of the system used was shown in a previous study [20]. The droplets were generated by a 1.7 MHz ultrasonic spray generator that consisted of six resonators, and then carried into the high-temperature diffusion flame by oxygen, the carrier gas. The flame nozzle had five concentric pipes, and the droplets generated from the precursor solution were transported to the diffusion flame by the flow of the carrier gas through the center pipe. The flow rates of the fuel, oxidizer, and carrier gas were 5, 40, and 8 L min^{-1}, respectively. Furthermore, the concentrations of the cobalt nitrate hexahydrate [$Co(NO_3)_2 \cdot 6H_2O$, Junsei] and tetraethyl orthosilicate [$Si(OC_2H_5)_4$, Samchun] solutions used were 0.08 and 0.005 M, respectively. A small volume of nitric acid was added in order to form the clear spray solution. Moreover, ethyl alcohol was added in order to increase the temperature of the diffusion flame; the volume ratio of ethyl alcohol to distilled water in the mixed solvent was 1:3. The filled Co@Si–CoO nanopowder was obtained by subjecting the filled Si–CoO nanopowder to a reduction process at 500 °C under a 10% H_2/Ar reducing atmosphere. The hollow Si–Co_3O_4 nanospheres were subsequently produced by oxidizing the filled Co@Si–CoO nanopowder at 300 °C for 3 h under an air atmosphere. The oxidation of undoped and SiO_2-doped filled CoO nanopowders, which were prepared by FSP, at 300 °C under an air atmosphere produced undoped and SiO_2-doped filled Co_3O_4 nanopowders. For simplicity, the SiO_2-doped Co_3O_4 nanospheres with hollow and solid structures, and undoped Co_3O_4 nanopowder with a solid structure will be referred to as "hollow Si–Co_3O_4" and "filled Si–Co_3O_4" nanospheres, and "undoped Co_3O_4" nanopowder, respectively.

The crystal structures of the powders were investigated via X-ray diffraction (XRD, X'pert PRO MPD) with Cu Kα radiation (λ = 1.5418 Å) at the Korea Basic Science Institute (Daegu). The morphologies of the powders were investigated via field-emission scanning electron microscopy (FE-SEM, Hitachi S-4800) and high-resolution transmission electron microscopy (HR-TEM, JEOL JEM-2100F) at a working voltage of 200 kV. The specific surface areas of the powders were calculated from the Brunauer-Emmett-Teller (BET) analysis of nitrogen adsorption measurements (TriStar 3000).

The electrochemical properties of the powders were analyzed by constructing a 2032-type coin cell. The anode was prepared by mixing the active material, carbon black, and sodium carboxymethyl cellulose (CMC) in a weight ratio of 7:2:1. Li metal, a microporous polypropylene film, and a 1 M solution of $LiPF_6$ dissolved in a mixture of ethylene carbonate and dimethyl carbonate (FEC and DMC, respectively; 1:1 v/v) were used as the counter electrode, separator, and electrolyte, respectively. Furthermore, the discharge/charge characteristics of the samples were investigated by cycling at various current densities for potentials ranging from 0.001 to 3 V; cyclic voltammograms were measured at a scan rate of 0.07 mV s^{-1}. The discharge/charge characteristics and cyclic voltammograms were measured with a WBCS3000K8. Electrochemical impedance spectra were obtained by performing alternating current (AC) electrochemical impedance spectroscopy (EIS) at a voltage of 10 mV and frequencies ranging from 0.1 Hz to 1000 kHz (VersaStat 4, Ametek).

3. Results and discussion

The morphology of the filled Si–CoO nanopowder prepared via the one-pot FSP process is shown in Fig. 1. The low-resolution TEM images (Fig. 1(a) and (b)) show the slightly aggregated and well-faceted nanoparticles resulting from the high surface energy of the ultrafine nanopowder, which have sizes of 12–43 nm. The nanoparticles have a pure crystalline cubic CoO structure, as shown in the corresponding XRD pattern (Fig. 2). In addition, the rapid quenching of the nanopowder formed inside the high-temperature (>2500 °C) diffusion flame produced an oxygen-deficient cobalt oxide nanopowder. Although the peaks corresponding to the crystalline structure of the Si component are absent from the XRD pattern, the TEM image (Fig. 1(c)) shows the single-crystal structure of the nanopowder. In addition, the HR-TEM image (Fig. 1(d)) shows the 0.21-nm-spaced lattice fringes, which correspond to the (200) crystal plane of cubic CoO. During FSP, the composite nanopowder is formed by the nucleation and growth of the cobalt oxide and silicon oxide vapors. However, the phase-separated SiO_2 layer is absent from the HR-TEM image. Nevertheless, the XRD peaks of the filled Si–CoO nanopowder are shifted to slightly higher angles compared to those of cubic CoO (JCPDS card no. 78-0431). Doping the CoO crystal structure with Si results in the formation of a filled Si–CoO nanopowder inside the high-temperature diffusion flame. As the elemental mapping images (Fig. 1(e)) show, Si is uniformly distributed throughout the CoO nanoparticles.

The filled Si–CoO nanopowder prepared by FSP was post-treated at 500 °C for 3 h under a reducing atmosphere (10% H_2/Ar). The post-treated powder has a mixed crystal structure that consists of metallic Co and cubic CoO phases, as shown in Fig. 2. Therefore, because of the formation of metallic Co, which has a low melting point, the well-faceted filled Si–CoO nanoparticles that were prepared directly by FSP are transformed into spherical nanoparticles (Fig. 3(a) and (b)) during the reduction process. The TEM images (Fig. 3(b) and (c)) show the core-shell structure of these nanoparticles. Furthermore, HR-TEM images of the cores and shells of the nanoparticles (Fig. 3(c)) show clear 0.17- and 0.21-nm-sized lattice fringes, which correspond to the (200) crystal planes of metallic Co and cubic CoO, respectively. The phase separation of the Co and Si components during the reduction process of the nanopowder results in the formation of a core-shell structure, i.e., the reduced metallic Co accumulates in the core, whereas the unchanged SiO_2, which has a low interaction strength, moves towards the surface of the nanoparticles. The SiO_2 layer plays a key role in preventing the aggregation of the metallic Co nanoparticles during the reduction process, which have a low melting point. Exposing the core-shell-structured Co@Si–CoO nanoparticles to an air atmosphere after the reduction process causes the surface oxidation of the ultrafine nanopowder. During oxidation, the Co cations diffuse outwards into the amorphous SiO_2 layer and form CoO nanocrystals by combining with oxygen anions that diffuse inwards into the SiO_2 layer. Therefore, the nanoparticles shown in Fig. 3(c) have a core-shell structure with a filled Co@Si–CoO configuration; the CoO–SiO_2 shell is 5 nm thick. The CoO nanocrystals are embedded within the amorphous SiO_2 layer that covers the metallic Co nanoparticles. The selected-area electron diffraction (SAED) pattern (Fig. 3(d)) also shows the structure of the filled Co@Si–CoO nanoparticles and the mixed crystal structure of metallic Co and CoO. In addition, the core-shell-structured nanoparticles have an average size of 21 nm, as determined from the TEM image.

The nanopowder obtained via the reduction process was post-treated at 300 °C under an air atmosphere. As the corresponding XRD pattern in Fig. 2 shows, the oxidized nanopowder has a pure cubic spinel Co_3O_4 structure (JCPDS card no. 42-1467). The filled Co@Si–CoO nanoparticles were transformed into hollow Si–Co_3O_4 composite nanospheres (Fig. 4(a–c)) via a nanoscale Kirkendall diffusion process. The SAED pattern shown in Fig. S1 also confirms the formation of hollow Si–Co_3O_4 composite nanospheres after the

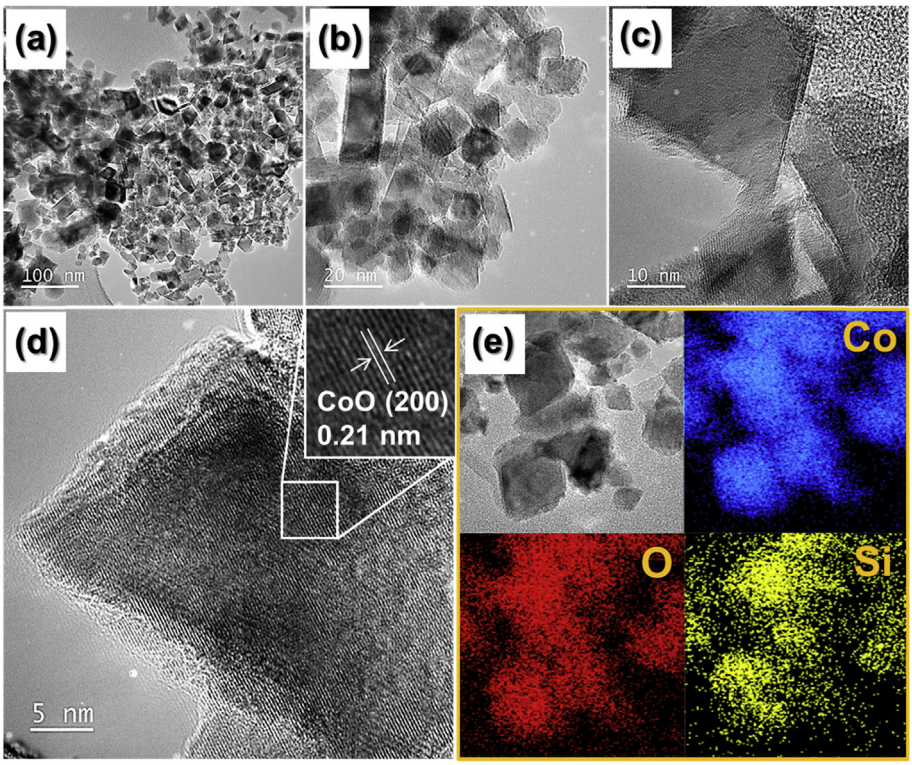

Fig. 1. TEM and elemental mapping images of the filled Si–CoO nanopowder prepared by FSP: (a–c) TEM, (d) HR-TEM, and (e) elemental mapping images.

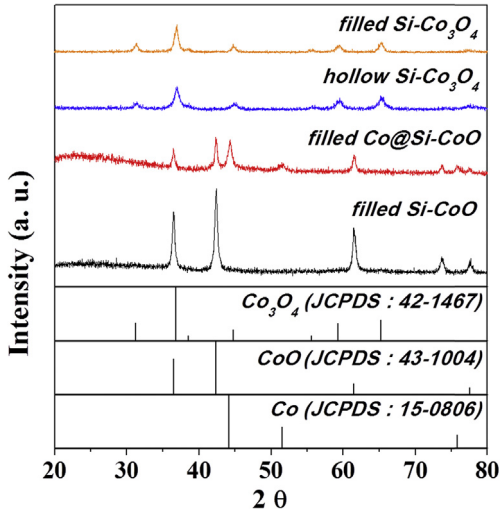

Fig. 2. XRD patterns of the nanopowders prepared by FSP before and after the post-treatment process.

oxidation process. The hollow shell is composed of ultrafine nanocrystals that are less than 10 nm in size, as revealed by the TEM images (Fig. 4(b) and (c)). Moreover, the 0.24-nm-spaced lattice fringes (Fig. 4(d)) correspond to the (311) crystal plane of the cubic spinel Co_3O_4 structure. The corresponding elemental mapping images (Fig. 4(e)) show that Co and Si are uniformly distributed over the surface of the hollow nanospheres. This is indicative of the formation of a solid solution of cobalt oxide and silicon oxide. The void spheres formed by nanoscale Kirkendall diffusion are indicated by the arrows in Fig. 4(e). Scheme 1 describes in detail the mechanism governing the formation of the hollow Si–Co_3O_4 nanospheres via the nanoscale Kirkendall diffusion process. The small Co cations diffuse towards the surface of the CoO–SiO_2 shell more rapidly than the oxygen anions diffuse inwards, thereby resulting in the formation of a CoO layer; the Co^{2+} cations and O^{2-} anions have ionic radii of 75 and 140 p.m., respectively. A Co_3O_4 layer then forms via the further oxidation of CoO during the diffusion process. In addition, metallic Co is fully transformed into cobalt oxide, and the SiO_2-doped Co_3O_4 structure produces the hollow Si–Co_3O_4 nanospheres; the nanospheres have a mean size of 42 nm, as determined from the TEM image. On the other hand, a filled Si–Co_3O_4 nanopowder (Fig. 1 and Fig. S2) was formed through the direct oxidation of the filled Si–CoO nanopowder, which was prepared by FSP, at 300 °C under an air atmosphere. This nanopowder is composed of ultrafine Co_3O_4 nanocrystals, as shown in the TEM image (Fig. S2(b)), that result from the oxidation-induced transformation of the SiO_2-doped CoO single crystals. The oxidation of the undoped CoO nanopowder, which was also prepared by FSP, at 300 °C under an air atmosphere produced an undoped Co_3O_4 nanopowder with a solid structure, as shown in Figs. S3 and S4. The filled and hollow Si–Co_3O_4 nanospheres, and undoped Co_3O_4 nanopowder had mean crystallite sizes of 10.9, 14.6, and 13.1 nm, respectively, as calculated from the half-width of the (311) peak by using the Scherrer equation.

The electrochemical properties of the SiO_2-doped Co_3O_4 and CoO nanopowders were investigated via cyclic voltammetry (CV) and galvanostatic charge/discharge measurements in order to determine their suitability for Li-ion storage. The CV curves of the first four cycles (Fig. 5) were obtained at a scan rate of 0.07 mV s^{-1} over voltages ranging from 0.001 to 3 V. At approximately 0.5 V in the first cathodic sweep, the filled Si–CoO nanopowder exhibits a sharp reduction peak because of the conversion reaction between CoO and Li^+, which produces metallic Co and Li_2O [35,36]. The hollow and filled Si–Co_3O_4 nanopowders exhibit sharp reduction peaks at approximately 0.9 V in the first cathodic sweep. These

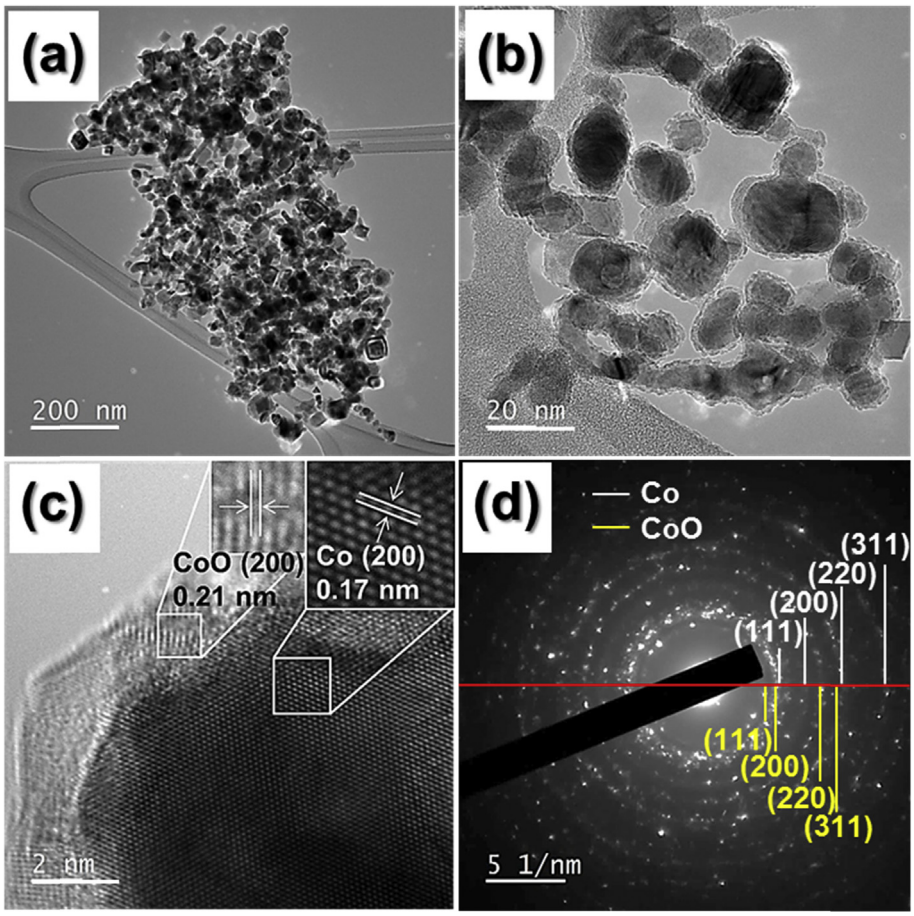

Fig. 3. TEM images and SAED pattern of the filled Co@Si–CoO nanopowders post-treated at 500 °C in a 10% H_2/Ar atmosphere for 3 h: (a, b) TEM images, (c) HR-TEM image, and (d) SAED pattern.

peaks result from the conversion reaction between Co_3O_4 and Li^+, which leads to the formation of metallic Co and Li_2O [37,38]. The sharp reduction peaks in the curves correspond to the dominant voltage plateaus that occur at approximately 0.6 and 1.0 V in the first discharge curves (Fig. 5(d)) of the SiO_2-doped CoO and Co_3O_4 nanopowders, respectively. Furthermore, the oxidation peaks of the SiO_2-doped Co_3O_4 and CoO nanopowders at approximately 2.1 V are attributed to the oxidation of metallic Co to CoO and the decomposition of Li_2O [35–38]. Broad reduction peaks are present at approximately 0.9 and 1.2 V from the second cycle onwards of the SiO_2-doped Co_3O_4 and CoO nanopowders. These peaks are attributed to the insertion of Li^+ into CoO and the conversion reaction between CoO and Li^+ that forms metallic Co and Li_2O, respectively. The strong overlapping of the CV profiles from the second cycle onwards (Fig. 5(c)) is evidence of the superior cycling ability of the hollow Si–Co_3O_4 nanospheres obtained through nanoscale Kirkendall diffusion. The hollow and filled Si–Co_3O_4 nanopowders exhibit initial discharge capacities of 1106 and 1139 mA h g^{-1}, respectively, at a high current density of 2 A g^{-1}; the corresponding initial Coulombic efficiencies are 75.7% and 82.4%, respectively. The filled Si–CoO nanopowder exhibits initial discharge and charge capacities of 1103 and 834 mA h g^{-1}, respectively. The high, initial, irreversible capacity loss of the filled Si–CoO and Si–Co_3O_4 nanopowders is attributed to the loss of structural stability during the first cycle; this loss stems from the significant volume changes that accompany Li insertion and desertion processes. Fig. 6(a) compares the cycling performance of all three SiO_2-doped samples at a high current density of 2 A g^{-1}. Fig. 6(a) shows that the hollow Si–Co_3O_4 nanospheres obtained through nanoscale Kirkendall diffusion exhibit superior cycling performance compared to that of the filled Si–CoO and Si–Co_3O_4 nanopowders. The capacity fade of the solid nanopowders is attributed to their gradual destruction following repeated Li insertions and desertions. Moreover, the hollow Si–Co_3O_4 nanopowder has a maximum 150th-cycle discharge capacity of 971 mA h g^{-1} and capacity retention of 99.5%, which was measured relative to the second cycle. However, the filled Si–CoO and Si–⊜ Co_3O_4 nanopowders have corresponding capacity retentions of only 82.2% and 71.5%, respectively. Fig. 6(b) shows the rate performance of the nanopowders for stepwise increases in the current density (0.5–3 A g^{-1}), with 10 cycles performed at each step. The hollow Si–Co_3O_4 nanopowder achieves reversible discharge capacities of 1062, 1022, 981, 938, 900, and 853 mA h g^{-1} after 10 cycles at current densities of 0.5, 1, 1.5, 2, 2.5, and 3 A g^{-1}, respectively. That is, the capacity decreases slightly as the current density increases from 0.5 to 3 A g^{-1}. In addition, with a value of 1060 mA h g^{-1}, the capacity almost completely recovers when the current density is returned to 0.5 A g^{-1}. The hollow Si–Co_3O_4 nanospheres also have superior cycling and rate performances compared to those of the solid, undoped, Co_3O_4 nanopowder, as shown in Fig. 6 and Fig. S5.

The superior Li-ion storage properties of the hollow Si–Co_3O_4 nanopowder compared to those of the other nanopowders was also confirmed by EIS analysis before and after 1 and 10 cycles. The compressed semi-circle in the high-medium frequency region of the Nyquist plots (Fig. 6(c–e)) represents the charge-transfer

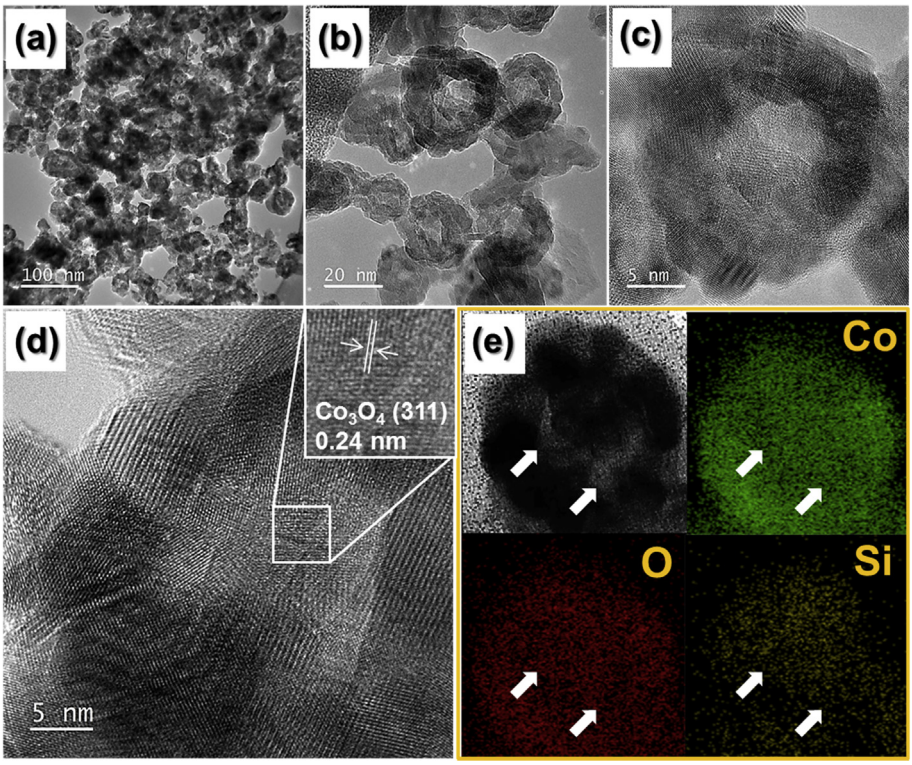

Fig. 4. TEM images of the hollow Si–Co_3O_4 nanospheres obtained after an oxidation time of 3 h in an air atmosphere: (a, b) TEM, (c) HR-TEM, and (d) elemental mapping images.

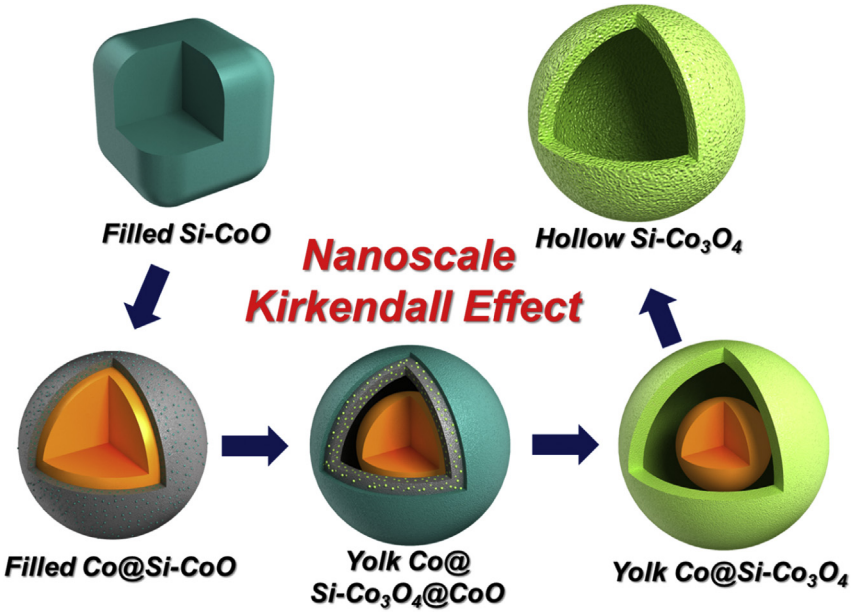

Scheme 1. Schematic diagram showing the formation mechanism of the hollow Si–Co_3O_4 nanospheres via the nanoscale Kirkendall diffusion process.

resistance (R_{ct}) of the electrode [39–41]. As Fig. 6(c) shows, the filled Si–CoO nanopowder has a lower R_{ct} value before cycling than that of the Si–Co_3O_4 counterpart. The R_{ct} values of all three samples decrease after the first cycle (Fig. 6(d)) because of the conversion of the nanopowders to ultrafine nanocrystals. Furthermore, Fig. 6(e) shows that the nanopowders that maintain a high structural stability during the repeated Li insertion and desertion processes have low R_{ct} values, which are similar to that of the filled Si–CoO nanopowder after 10 cycles. However, the R_{ct} value of the filled Si–Co_3O_4 nanopowder increases after 10 cycles. Furthermore, the steep line in the low-frequency region shown in Fig. 6(d) and (e) is indicative of the high Li-ion conductivity of the hollow nanopowder. Therefore, the high structural stability during cycling and high Li-ion conductivity, which are caused by the hollow structure, are responsible for the excellent Li-ion storage properties of the hollow Si–Co_3O_4 nanospheres obtained via nanoscale Kirkendall

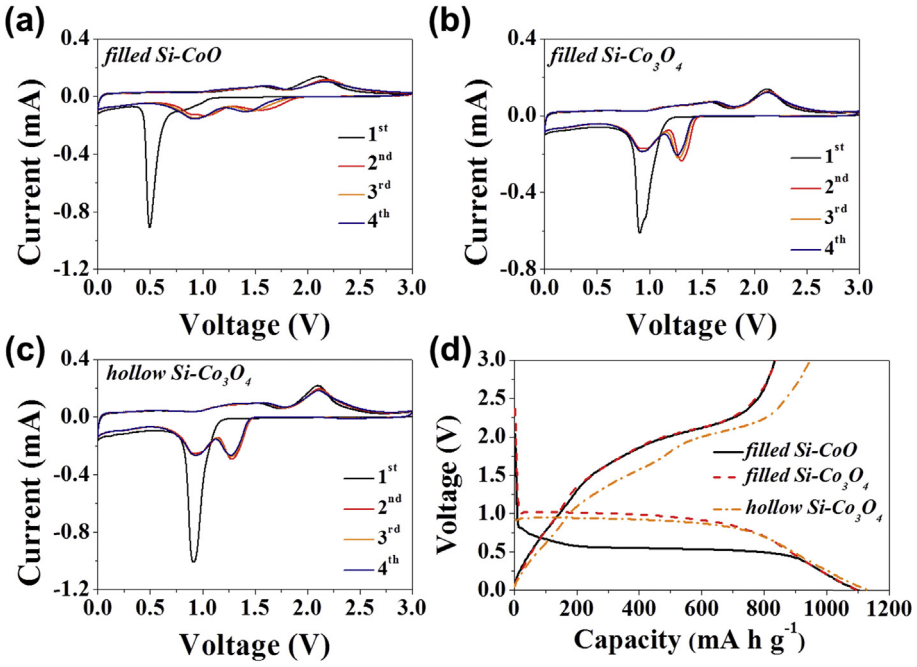

Fig. 5. CV, initial charge, and initial discharge curves of the three samples: (a) CV curves of the filled Si–CoO nanopowder, (b) CV curves of the filled Si–Co_3O_4 nanopowder, (c) CV curves of the hollow Si–Co_3O_4 nanopowder, and (d) initial charge and discharge curves of the three samples.

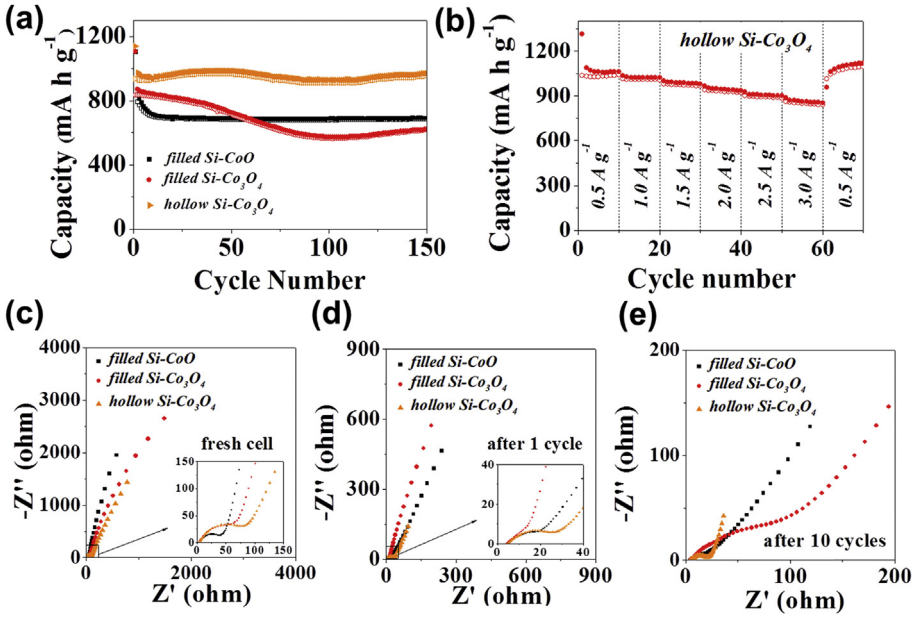

Fig. 6. Cycling and rate performances, and Nyquist plots of the three samples: (a) cycling performances, (b) rate performance, (c) Nyquist plots before cycling, (d) Nyquist plots after 1 cycle, and (e) Nyquist plots after 10 cycles.

diffusion.

4. Conclusions

The mechanism governing the formation of hollow Si–Co_3O_4 nanospheres by applying a nanoscale Kirkendall diffusion process was investigated. Solid metallic Co nanoparticles that were covered with a SiO_2 layer, which was formed as an intermediate product, were transformed into hollow Si–Co_3O_4 nanospheres. The SiO_2 layer was formed during the reduction process, and it played a key role in the preparation of the aggregate-free, hollow, Si–Co_3O_4 nanospheres. The hollow Si–Co_3O_4 nanospheres exhibited high structural stability, high Li-ion conductivity, and superior electrochemical properties for Li-ion storage compared to the filled Si–CoO and Si–Co_3O_4 nanopowders. More importantly, the simple process applied in this study is generally applicable to the preparation of SiO_2-doped, hollow, metal oxide nanopowders from solid, SiO_2-doped, metal oxide nanopowders formed by a FSP process.

Acknowledgment

This work was supported by a National Research Foundation of Korea (NRF) grant funded by the Korean government (MEST) (NRF-2015R1A2A1A15056049).

Appendix A. Supplementary data

Supplementary data related to this article can be found at http://dx.doi.org/10.1016/j.jallcom.2016.04.104.

References

[1] L. Kang, D. He, L. Bie, P. Jiang, Nanoporous cobalt oxide nanowires for non-enzymatic electrochemical glucose detection, Sens. Actuator B Chem. 220 (2015) 888–894.
[2] J.W. Yoon, Y.J. Hong, G.D. Park, S.J. Hwang, F. Abdel-Hady, A.A. Wazzan, Y.C. Kang, J.H. Lee, Kilogram-scale synthesis of Pd-loaded quintuple-shelled Co_3O_4 microreactors and their application to ultrasensitive and ultraselective detection of methylbenzenes, ACS Appl. Mater. Interfaces 7 (2015) 7717–7723.
[3] C.S. Li, G. Melaet, W.T. Ralston, K. An, C. Brooks, Y. Ye, Y.S. Liu, J. Zhu, J. Guo, S. Alayoglu, G.A. Somorjai, High-performance hybrid oxide catalyst of manganese and cobalt for low-pressure methanol synthesis, Nat. Commun. 6 (2015) 6538.
[4] H. Jin, J. Wang, D. Su, Z. Wei, Z. Pang, Y. Wang, In situ cobalt–cobalt oxide/N-doped carbon hybrids as superior bifunctional electrocatalysts for hydrogen and oxygen evolution, J. Am. Chem. Soc. 137 (2015) 2688–2694.
[5] Y. Liang, Y. Li, H. Wang, J. Zhou, J. Wang, T. Rengier, H. Dai, Co_3O_4 nanocrystals on graphene as a synergistic catalyst for oxygen reduction reaction, Nat. Mater. 10 (2011) 780–786.
[6] P. Poizot, S. Laruelle, S. Grugeon, L. Dupont, J.M. Tarascon, Nano-sized transition-metal oxides as negative-electrode materials for lithium-ion batteries, Nature 407 (2000) 496–499.
[7] Z. Wang, H. Bi, P. Wang, M. Wang, Z. Liu, L. Shen, X. Liu, Magnetic and microwave absorption properties of self-assemblies composed of core–shell cobalt–cobalt oxide nanocrystals, Phys. Chem. Chem. Phys. 17 (2015) 3796–3801.
[8] Y.J. Kim, J.H. Lee, S.G. Cho, Y.W. Kwon, I. In, J.H. Lee, N.H. You, E. Reichmanis, H.D. Ko, K.T. Lee, H.K. Kwon, D.H. Ko, H.S. Yang, B.N. Park, Additive-free hollow-structured Co_3O_4 nanoparticle Li-ion battery: the origins of irreversible capacity loss, ACS Nano 8 (2014) 6701–6712.
[9] L. Tao, J. Zaia, K. Wang, H. Zhang, M. Xu, J. Shen, Y. Su, X. Qian, Co_3O_4 nanorods/graphene nanosheets nanocomposites for lithium ion batteries with improved reversible capacity and cycle stability, J. Power Sources 202 (2012) 230–235.
[10] G.D. Park, J.H. Lee, J.K. Lee, Y.C. Kang, Effect of esterification reaction of citric acid and ethylene glycol on the formation of multi-shelled cobalt oxide powders with superior electrochemical properties, Nano Res. 7 (2014) 1738–1748.
[11] J. Wang, N. Yang, H. Tang, Z. Dong, Q. Jin, M. Yang, D. Kisailus, H. Zhao, Z. Tang, D. Wang, Accurate control of multishelled Co_3O_4 hollow microspheres as high-performance anode materials in lithium-ion batteries, Angew. Chem. 125 (2013) 6545–6548.
[12] D. Gu, W. Li, F. Wang, H. Bongard, B. Spliethoff, W. Schmidt, C. Weidenthaler, Y. Xia, D. Zhao, F. Schith, Controllable synthesis of mesoporous peapod-like Co_3O_4@Carbon nanotube arrays for high-performance lithium-ion batteries, Angew. Chem. Int. Ed. 54 (2015) 7060–7064.
[13] H. Wu, M. Xu, Y. Wang, G. Zheng, Branched Co_3O_4/Fe_2O_3 nanowires as high capacity lithium-ion battery anodes, Nano Res. 6 (2013) 167–173.
[14] H. Wang, N. Mao, J. Shi, Q. Wang, W. Yu, X. Wang, Cobalt oxide-carbon nanosheet nanoarchitecture as an anode for high-performance lithium-ion battery, ACS Appl. Mater. Interfaces 7 (2015) 2882–2890.
[15] Z.S. Wu, W. Ren, L. Wen, L. Gao, J. Zhao, Z. Chen, G. Zhou, F. Li, H.M. Cheng, Graphene anchored with Co_3O_4 nanoparticles as anode of lithium ion batteries with enhanced reversible capacity and cyclic performance, ACS Nano 4 (2010) 3187–3194.
[16] G.D. Park, J.S. Cho, Y.C. Kang, Novel cobalt oxide-nanobubble-decorated reduced graphene oxide sphere with superior electrochemical properties prepared by nanoscale Kirkendall diffusion process, Nano Energy 17 (2015) 17–26.
[17] D. Tian, X.L. Zhou, Y.H. Zhang, Z. Zhou, X.H. Bu, MOF-derived porous Co_3O_4 hollow tetrahedra with excellent performance as anode materials for lithium-ion batteries, Inorg. Chem. 54 (2015) 8159–8161.
[18] D. Li, D. Shi, Z. Chen, H. Liu, D. Jiac, Z. Guo, Enhanced rate performance of cobalt oxide/nitrogen doped graphene composite for lithium ion batteries, RSC Adv. 3 (2013) 5003–5008.
[19] P. Roy, S.K. Srivastava, Nanostructured anode materials for lithium ion batteries, J. Mater. Chem. A 3 (2015) 2454–2484.
[20] Z. Wang, L. Zhou, X.W. Lou, Metal oxide hollow nanostructures for lithium-ion batteries, Adv. Mater. 24 (2012) 1903–1911.
[21] Y.J. Hong, M.Y. Son, Y.C. Kang, One-pot facile synthesis of double-shelled SnO_2 yolk-shell-structured powders by continuous process as anode materials for Li-ion batteries, Adv. Mater. 25 (2013) 2279–2283.
[22] F. Cheng, J. Liang, Z. Tao, J. Chen, Functional materials for rechargeable batteries, Adv. Mater. 23 (2011) 1695–1715.
[23] L. Mai, X. Tian, X. Xu, L. Chang, L. Xu, Nanowire electrodes for electrochemical energy storage devices, Chem. Rev. 114 (2014) 11828–11862.
[24] W.Y. Teoh, R. Amal, L. Mädler, Flame spray pyrolysis: an enabling technology for nanoparticles design and fabrication, Nanoscale 2 (2010) 1324–1347.
[25] K.D. Kim, S. Pokhrel, Z. Wang, H. Ling, C. Zhou, Z. Liu, M. Hunger, L. Mädler, J. Huang, Tailoring high-performance Pd catalysts for chemoselective hydrogenation reactions via optimizing the parameters of the double-flame spray pyrolysis, ACS Catal. 6 (2016) 2372–2381.
[26] K. Inyawilert, D. Channei, N. Tamaekong, C. Liewhiran, A. Wisitsoraat, A. Tuantranont, S. Phanichphant, Pt-doped In_2O_3 nanoparticles prepared by flame spray pyrolysis for NO_2 sensing, J. Nanoparticle Res. (2016), http://dx.doi.org/10.1007/s11051-016-3341-1.
[27] Y.C. Kang, D.J. Seo, S.B. Park, H.D. Park, Direct synthesis of strontium titanate phosphor particles with high luminescence by frame spray pyrolysis, Mater. Res. Bull. 37 (2002) 263–269.
[28] D. Li, W.Y. Teoh, C. Selomulya, R.C. Woodward, P. Munroed, R. Amal, Insight into microstructural and magnetic properties of flame-made γ-Fe_2O_3 nanoparticles, J. Mater. Chem. 17 (2007) 4876–4884.
[29] J.H. Kim, J.H. Yi, Y.N. Ko, Y.C. Kang, Electrochemical properties of nano-sized $LiNi_{1/3}Co_{1/3}Mn_{1/3}O_2$ powders in the range from 56 to 101 nm prepared by flame spray pyrolysis, Mater. Chem. Phys. 134 (2012) 254–259.
[30] J.M. Won, J.H. Kim, Y.J. Choi, J.S. Cho, Y.C. Kang, Design and synthesis of metal oxide hollow nanopowders for lithium-ion batteries by combining nanoscale Kirkendall diffusion and flame spray pyrolysis, Ceram. Int. 42 (2016) 5461–5471.
[31] S.H. Choi, J.H. Lee, Y.C. Kang, One-pot rapid synthesis of core–shell structured NiO@TiO_2 nanopowders and their excellent electrochemical properties as anode materials for lithium ion batteries, Nanoscale 5 (2013) 12645–12650.
[32] J.H. Kim, J.H. Lee, Y.C. Kang, Flame spray pyrolysis for finding multicomponent nanomaterials with superior electrochemical properties in the CoO_x-FeO_x system for use in lithium-ion batteries, Chem. Asian J. 9 (2014) 2826–2830.
[33] S.H. Choi, Y.C. Kang, Characteristics of $ZnMn_2O_4$ nanopowders prepared by flame spray pyrolysis for use as anode material in lithium ion batteries, Int. J. Electrochem. Sci. 8 (2013) 6281–6290.
[34] G.D. Park, S.H. Choi, Y.C. Kang, Electrochemical properties of ultrafine TiO_2-doped MoO_3 nanoplates prepared by one-pot flame spray pyrolysis, RSC Adv. 4 (2014) 17382–17386.
[35] A.K. Rai, L.T. Anh, J.H. Gim, J.K. Kim, One-step synthesis of CoO anode material for rechargeable lithium-ion batteries, Ceram. Int. 39 (2013) 9325–9330.
[36] W. Yao, J. Chen, H. Cheng, Platelike CoO/carbon nanofiber composite electrode with improved electrochemical performance for lithium ion batteries, J. Solid State Electrochem. 15 (2011) 183–188.
[37] G. Huang, S. Xu, S. Lu, L. Li, H. Sun, Micro-/Nanostructured Co_3O_4 anode with enhanced rate capability for lithium-ion batteries, ACS Appl. Mater. Interfaces 6 (2014) 7236–7243.
[38] H. Sun, X. Sun, T. Hu, M. Yu, F. Lu, J. Lian, Graphene-wrapped mesoporous cobalt oxide hollow spheres anode for high-rate and long-life lithium ion batteries, J. Phys. Chem. C 118 (2014) 2263–2272.
[39] M.M. Rahman, I. Sultana, Z. Chen, M. Srikanth, L.H. Li, X.J. Dai, Y. Chen, *Ex situ* electrochemical sodiation/desodiation observation of Co_3O_4 anchored carbon nanotubes: a high performance sodium-ion battery anode produced by pulsed plasma in a liquid, Nanoscale 7 (2015) 13088–13095.
[40] G. Li, L. Xu, Q. Hao, M. Wang, Y. Qian, Synthesis, characterization and application of carbon nanocages as anode materials for high-performance lithium-ion batteries, RSC Adv. 2 (2012) 284–291.
[41] Y. Shi, J.Z. Wang, S.L. Chou, D. Wexler, H.J. Li, K. Ozawa, H.K. Liu, Y.P. Wu, Hollow structured Li_3VO_4 wrapped with graphene nanosheets in situ prepared by a one-pot template-free method as an anode for lithium-ion batteries, Nano Lett. 13 (2013) 4715–4720.